



**Climatological characteristics of
raindrop size distributions**

S.-H. Suh et al.

This discussion paper is/has been under review for the journal Hydrology and Earth System Sciences (HESS). Please refer to the corresponding final paper in HESS if available.

Climatological characteristics of raindrop size distributions within a topographically complex area

S.-H. Suh¹, C.-H. You², and D.-I. Lee^{1,2}

¹Department of Environmental Atmospheric Sciences, Pukyong National University, Daeyeon campus 45, Yongso-ro, Namgu, Busan 608-737, Republic of Korea

²Atmospheric Environmental Research Institute, Daeyeon campus 45, Yongso-ro, Namgu, Busan 608-737, Republic of Korea

Received: 17 March 2015 – Accepted: 30 March 2015 – Published: 20 April 2015

Correspondence to: C.-H. You (youch@pknu.ac.kr)

Published by Copernicus Publications on behalf of the European Geosciences Union.

Title Page

Abstract

Introduction

Conclusions

References

Tables

Figures



Back

Close

Full Screen / Esc

Printer-friendly Version

Interactive Discussion



Abstract

Raindrop size distribution (DSD) characteristics within the complex area of Busan, Korea (35.12° N, 129.10° E) were studied using a Precipitation Occurrence Sensor System (POSS) disdrometer over a four-year period from 24 February 2001 to 24 December 2004. Average DSD parameters in Busan, a mid-latitude site, were compared with corresponding parameters recorded in the high-latitude site of Järvenpää, Finland. Mean values of median drop diameter (D_0) and the shape parameter (μ) in Busan are smaller than those in Järvenpää, whereas the mean normalized intercept parameter (N_w) and rainfall rate (R) are higher in Busan.

To analyze the climatological DSD characteristics in more detail, the entire period of recorded rainfall was divided into 10 categories with different temporal and spatial scales. When only convective rainfall was considered, mean D_m and N_w values for all these categories converged around a maritime cluster, except for rainfall associated with typhoons. The convective rainfall of a typhoon showed much smaller D_m and larger N_w compared with the other rainfall categories.

In terms of diurnal DSD variability, we observe maritime (continental) precipitation during the daytime (DT) (nighttime, NT), which likely results from sea (land) breeze identified through wind direction analysis. These features also appeared in the seasonal diurnal distribution. The DT and NT Probability Density Function (PDF) during the summer was similar to the PDF of the entire study period. However, the DT and NT PDF during the winter season displayed an inverse distribution due to seasonal differences in wind direction.

1 Introduction

Drop Size Distribution (DSD) controls microphysical processes of rainfall and therefore plays an important role in the development of quantitative rainfall estimation algorithms based on forward scattering simulations of radar measurements

HESSD

12, 4005–4045, 2015

Climatological characteristics of raindrop size distributions

S.-H. Suh et al.

Title Page

Abstract

Introduction

Conclusions

References

Tables

Figures

⏪

⏩

◀

▶

Back

Close

Full Screen / Esc

Printer-friendly Version

Interactive Discussion



Climatological characteristics of raindrop size distributions

S.-H. Suh et al.

Title Page

Abstract

Introduction

Conclusions

References

Tables

Figures

⏪

⏩

◀

▶

Back

Close

Full Screen / Esc

Printer-friendly Version

Interactive Discussion



(Seliga and Bringi, 1976). DSD data accurately reflect local rainfall characteristics within an observation area (You et al., 2014). Many DSD models have been developed to characterize spatial–temporal differences in DSDs under various atmospheric conditions (Ulbrich, 1983). Marshall and Palmer (1948) developed an exponential DSD model using DSD data collected by a filter paper technique ($N(D) = 8 \times 10^3 \exp(-410R^{-0.21}D)(m^{-3} mm^{-1})$). In subsequent studies, a lognormal distribution was assumed to overcome the problem of exponential DSD mismatching with real data (Mueller, 1966; Levin, 1971; Markowitz, 1976; Feingold and Levin, 1986).

To further investigate natural DSD variations, Ulbrich (1983) developed a gamma DSD that permitted changing the dimension of the intercept parameter of $N_0(m^{-3} mm^{-1-\mu})$ with ($N(D) = N_0 D^\mu \exp(-\Lambda D)$). In addition, to enable the quantitative analysis of different rainfall events, the development of a normalized gamma DSD model that accounted for the independent spread of DSD from the disdrometer channel interval enabled a better representation of the actual DSD (Willis, 1984; Dou et al., 1999; Testud et al., 2001).

DSDs depend on the rainfall type, geographical and atmospheric conditions, and observation time, and are closely linked to microphysical characteristics that control rainfall development mechanisms. The microphysical structures of rainfall are more complicated in the middle and high latitudes than in the low latitudes (Leinonen et al., 2012).

In the case of stratiform rainfall, raindrops grow by accretion because of the relatively long residence time in weak updrafts, in which almost all water droplets are changed to ice particles. With time, the ice particles grow sufficiently and fall to ground. The raindrop size of stratiform rainfall observed at ground level is larger than that of convective rainfall, due to the resistance of the ice particles to break-up mechanisms. In contrast to stratiform rainfall, in convective rainfall raindrops grow by the collision-coalescence mechanism associated with relatively strong vertical wind speeds and short residence time in the cloud. Fully-grown raindrops are smaller in diameter than those in stratiform rainfall due to the break-up mechanism (Mapes and Houze Jr, 1993; Tokay and Short,

stratiform/convective and continental/maritime rainfall, and discuss diurnal variations. Finally, a summary of the results and the main conclusions are presented in Sect. 4.

2 Data and methods

2.1 Normalized gamma DSD

5 The DSD reflects the microphysical characteristics of rainfall. Normalization is used to define the DSD and to solve the non-independence of each DSD parameter (Willis, 1984; Dou et al., 1999; Testud et al., 2001). Furthermore, a normalized gamma DSD enables the comparison of quantitative estimations for cases of rainfall events that have different time scales and rain rates. Here, we use the DSD model designed by Testud
10 et al. (2001):

$$N(D) = N_w f(\mu) \left(\frac{D}{D_m} \right)^\mu \exp \left[- (4 + \mu) \frac{D}{D_m} \right] \quad (1)$$

where $N(D)$ is the number concentration ($\text{m}^{-3} \text{mm}^{-1}$), D is raindrop size (mm), and $f(\mu)$ is defined using the shape parameter (μ) and gamma function (Γ) as follows:

$$f(\mu) = \frac{6 (\mu + 4)^{4+\mu}}{4^4 \Gamma(4 + \mu)} \quad (2)$$

15 From the value of $N(D)$, the median volume diameter D_0 can be obtained as follows:

$$\int_0^{D_0} D^3 N(D) dD = \frac{1}{2} \int_0^{D_{\max}} D^3 N(D) dD \quad (3)$$

Title Page

Abstract

Introduction

Conclusions

References

Tables

Figures

⏪

⏩

◀

▶

Back

Close

Full Screen / Esc

Printer-friendly Version

Interactive Discussion



Mass-weighted mean diameter (D_m) is calculated as the ratio of the fourth to the third moment of the DSD:

$$D_m = \frac{\int_0^{D_{\max}} D^3 N(D) dD}{\int_0^{D_{\max}} D^4 N(D) dD} \quad (4)$$

The normalized intercept parameter (N_w) is calculated as follows:

$$N_w = \frac{4^4}{\pi \rho_w} \left(\frac{\text{LWC}}{D_m^4} \right) \quad (5)$$

The shape of the DSD is calculated as the ratio of D_m to the SD of D_m (Ulbrich and Atlas, 1998; Bringi et al., 2003; Leinonen et al., 2012):

$$\frac{\sigma_m}{D_m} = \left[\frac{\int_0^{D_{\max}} D^3 (D - D_m)^2 N(D) dD}{\int_0^{D_{\max}} D^3 N(D) dD} \right]^{1/2} \quad (6)$$

In addition, σ_m/D_m is related to μ as follows:

$$\frac{\sigma_m}{D_m} = \frac{1}{(4 + \mu)^{1/2}} \quad (7)$$

Liquid water content (LWC) and rainrate (R) can be defined from the estimated DSD:

$$\text{LWC} = \frac{\pi}{6} \rho_w \int_0^{D_{\max}} D^3 N(D) dD \quad (8)$$

where ρ_w is water density (gm^{-3}). Similarly, R can be defined as follows:

$$R = \frac{3.6 \pi}{10^3 6} \int_0^{D_{\max}} \rho_w N(D) dD \quad (9)$$

where $v(D)$ is the fall velocity for each raindrop size. The relationship between fall velocity (ms^{-1}) and raindrop size (D) is given by Atlas et al. (1973) who developed an empirical formula based on the data reported by Gunn and Kinzer (1949):

$$v(D) = 9.65 - 10.3 \exp[-0.6D] \quad (10)$$

2.2 Quality control of POSS data

POSS was used to measure the number of raindrops within the diameter range of 0.34–5.34 mm, using bistatic, continuous wave X-band Doppler radar across 34 channels (Fig. 1; Sheppard and Joe, 2008).

A POSS disdrometer was installed in Busan, Korea, along with other atmospheric instruments, the locations of which are shown in Fig. 2. Estimating raindrop size correctly is challenging and care should be taken to ensure reliable data are collected. We performed the following quality controls to optimize the accuracy of the disdrometer estimates. (i) Snow event data detected by POSS were excluded, to focus only on liquid state rainfall. (ii) Non-atmospheric data were removed from the analysis if the DSD spectra was smaller than five consecutive channels, or smaller (larger) than the 5th (10th) channel. (iii) Only data recorded in more than 10 complete channels were considered. (iv) To compensate for the reduced capability to detect raindrops smaller than 1 mm when $R > 200 \text{ mm h}^{-1}$ (as recorded by the disdrometer), data collected when $R > 200 \text{ mm h}^{-1}$ were not included in the analyses. (v) To eliminate wind and acoustic noise, data collected when $R < 0.1 \text{ mm h}^{-1}$ were removed (Tokay and Short, 1996). (vi) The DSD tends to be overestimated when $D_m < 0.5 \text{ mm}$ (Leinonen et al., 2012). Because the correlation coefficient between D_0 and D_m was 0.985 for the whole study period, we considered that D_m could be used for the analysis instead of D_0 . After performing all quality control procedures, 114 155 spectra were left from an original total of 166 682. Accumulated rainfall amount from POSS during the entire period was about 4269 mm. To verify the reliability of the POSS data, they were compared with data collected by a 0.5 mm tipping bucket rain gauge at an automatic weather system (AWS) located $\sim 368 \text{ m}$ from the POSS (Fig. 3).

2.3 Radar Parameters

To derive the rainfall relations, polarimetric parameters were computed by a T-matrix scattering simulation (Waterman, 1971; Zhang et al., 2001). The radar reflectivity factor (z , $\text{mm}^6 \text{m}^{-3}$) and horizontal polarized radar reflectivity (Z_h , dBZ) were computed using the DSD data collected by POSS, as follows:

$$z = \int_0^{D_{\max}} D^6 N(D) dD \quad (11)$$

$$Z_h = 10 \log_{10}(z) \quad (12)$$

Axis ratios of raindrops differ with atmospheric conditions and rainfall type. To derive the drop shape relation from the drop diameter, we performed numerical simulations and wind tunnel tests employing a fourth-polynomial equation, as in many previous studies (Beard and Chuang, 1987; Pruppacher and Beard, 1970; Andsager et al., 1999; Brandes et al., 2002). The drop-shape relation used in the present study is a combination of those from Andsager et al. (1999) and Beard and Chuang (1987) for three raindrop size ranges (Bringi et al., 2003).

The raindrop axis ratio relation of Andsager et al. (1999) is applied in the range of $1 < D(\text{mm}) < 4$, as follows:

$$r = 1.0048 + 0.0057D - 2.628D^2 + 3.682D^3 - 1.677D^4 \quad (13)$$

The drop-shape relation of Beard and Chuang (1987) is applied in the range of $D < 1 \text{ mm}$ and $D > 4 \text{ mm}$, as follows:

$$r = 1.012 + 0.01445D - 0.01028D^2 \quad (14)$$

We assumed the SD and the mean canting angle of raindrops as 7 and 0° , respectively. The refractive indices of liquid water at 20°C were used (Ray, 1972). We calculated dual

HESSD

12, 4005–4045, 2015

Climatological characteristics of raindrop size distributions

S.-H. Suh et al.

Title Page

Abstract

Introduction

Conclusions

References

Tables

Figures

⏪

⏩

◀

▶

Back

Close

Full Screen / Esc

Printer-friendly Version

Interactive Discussion



polarized radar parameters based on these conditions. The parameters of differential reflectivity, Z_{dr} (dB), specific differential phase, K_{dp} (deg km⁻¹), and attenuation, A_h (dB km⁻¹), using one-minute resolution DSD data were calculated and analyzed.

2.4 Classification of rainfall types and rainfall events

Rainfall systems can be classified as stratiform or convective in nature, via analysis of the following microphysical characteristics: (i) DSD, using relationships between N_0 and R ($N_0 = 4 \times 10^9 R^{4.3}$) (Tokay and Short, 1996; Testud et al., 2001), (ii) radar reflectivity, where, according to Gamadze and Houze (1982), a rainfall system that displays radar reflectivity larger than 38 dBZ is considered to be convective, and (iii) rainfall rate, where average 5 min $R > 0.5$ mm h⁻¹ is considered convective rainfall (Hamilton, 1988). Alternatively, rainfall that has 1 min $R > 5$ mm h⁻¹ and a SD of $R > 1.5$ is considered as convective type (Bringi et al., 2003). The rainfall classification method proposed by Bringi et al. (2003) is applied in the present study.

It is necessary to categorize different rainfall systems because their microphysical characteristics show great variation depending on the type of rainfall, as well as the type of rainfall event; e.g., typhoon, changma, heavy rainfall and seasonally discrete rainfall. To investigate the temporal variation in DSDs, we analyzed daily and seasonal DSDs. Likewise, to investigate diurnal variability in DSD, DT and NT data were considered by using the sunrise and sunset time in Busan (provided by the Korea Astronomy and Space Science Institute (KASI)). In the middle latitudes, and especially Busan, the timings of sunrise and sunset vary due to solar culminating height. The earliest and latest sunrise (sunset) time is 05:09 KST (17:12 KST) and 07:33 KST (19:42 KST), respectively. DT (NT) is defined as the period from the latest sunrise (sunset) time to the earliest sunset (sunrise) time (Table 1). To analyze the predominant characteristics of DSDs for typhoon rainfall, nine typhoon events were selected from throughout the entire study period.

HESSD

12, 4005–4045, 2015

Climatological characteristics of raindrop size distributions

S.-H. Suh et al.

Title Page

Abstract

Introduction

Conclusions

References

Tables

Figures

⏪

⏩

◀

▶

Back

Close

Full Screen / Esc

Printer-friendly Version

Interactive Discussion



This study utilizes the Korea Meteorological Administration (KMA) rainfall warning regulations to identify heavy rainfall events. The KMA issues a warning if the accumulated rain amount is expected to be $> 70 \text{ mm h}^{-1}$ within a 6 h period, or $> 110 \text{ mm h}^{-1}$ within a 12 h period. Rainfall events classified as changma and typhoon were not included in the classification “heavy rainfall”.

Changma is the rainfall system or rainy season that is usually present over the Korean Peninsula between mid-June and mid-July. The selected dates and periods of each rainfall category are summarized in Table 1.

3 Results

3.1 DSD and radar parameters

Figure 4 shows the Probability Density Function (PDF) and Cumulative Distribution Function (CDF) of DSDs and radar parameters with respect to stratiform and convective rainfall. The PDFs of DSD and radar parameters were calculated using the non-parameterization kernel estimation to identify the dominant distribution of each parameter recorded in Busan. Non-parameterization kernel estimation was also used to identify continuous distributions of DSDs. The PDF of stratiform rainfall is similar to that of the dataset for the entire analysis period due to the dominant contribution of stratiform rainfall (about 90.6%) to the overall rainfall. However, the PDF for convective rainfall is significantly different from that of the entire analysis period, and as the convective rainfall contributes only 5.8% of the overall rainfall (Table 4). When $\mu < 0$ the distribution of μ for convective rain is more frequent than that for stratiform rain (Fig. 4a). Alternatively, the frequency of μ for stratiform rainfall is higher than that of convective rainfall when $0 < \mu < 5$. The value of μ for convective rainfall is higher than that for stratiform rainfall because the break-up mechanism reduces the number concentration of large raindrops. As the result, the number concentrations of mid-size raindrops increased due to the decrease in the number concentration of relatively large

Title Page

Abstract

Introduction

Conclusions

References

Tables

Figures

⏪

⏩

◀

▶

Back

Close

Full Screen / Esc

Printer-friendly Version

Interactive Discussion



raindrops (Hu and Srivastava, 1995; Sauvageot and Lacaux, 1995). However, we observed a higher frequency of convective rainfall than stratiform rainfall in the negative μ range.

The PDF of D_m displays two peaks around 0.7 and 1.2 mm for stratiform rainfall and the entire rainfall dataset, respectively. We note that a gentle peak exists around 0.7 mm for both stratiform and convective rainfall datasets (Fig. 4b). These features are similar to the distribution of D_m observed in a high-latitude region at Järvenpää, Finland (Fig. 4 of Leinonen et al., 2012). For D_m values > 1.5 mm, the PDF for convective rainfall is higher than stratiform rainfall. Accordingly, the frequency of stratiform rainfall is higher than that of convective rainfall when $D_m < 1.5$ mm. Generally, stratiform rainfall that develops by the cold rain process displays weaker upward winds and less efficient break-up of raindrops. Therefore, stratiform rainfall tends to produce larger raindrops than convective rainfall that develops by the warm rain process. In contrast to this general concept, the average D_m values for convective and stratiform rain are approximately 1.6 and 1.3 mm, respectively. This finding is consistent with the results of Atlas et al. (1999) who found that the D_m of convective rainfall is larger than that of stratiform rainfall on Kapingamarangi Island, Micronesia.

The PDF of $\log_{10}(N_w)$ for the entire rainfall dataset was evenly distributed between 1.5 and 5.5 $\text{m}^{-3} \text{mm}^{-1}$, with a peak at $N_w = 3.3 \text{m}^{-3} \text{mm}^{-1}$ (Fig. 4c). The PDF of $\log_{10}(N_w)$ for stratiform rainfall is rarely $> 5.5 \text{m}^{-3} \text{mm}^{-1}$, while for convective rainfall it is often $> 5.5 \text{m}^{-3} \text{mm}^{-1}$. There is a similar frequency in the stratiform and convective rainfall at 4.4 $\text{m}^{-3} \text{mm}^{-1}$.

The PDF distributions for $\log_{10}(R)$ and $\log_{10}(\text{LWC})$ are similar (Fig. 4d and e). The PDF of $\log_{10}(R)$ for the entire rainfall dataset ranged between -1 and 2mm h^{-1} . A peak exists at 0.3mm h^{-1} and the PDF rapidly decreases from the peak value as R increases. The PDF for stratiform rainfall has a higher frequency than that of the entire rainfall when $\log(R) < 0.5 \text{mm h}^{-1}$, while the PDF for convective rainfall is denser between 0.4 and 2mm h^{-1} . Furthermore, at the peak value of 0.9mm h^{-1} , the fre-

HESSD

12, 4005–4045, 2015

Climatological characteristics of raindrop size distributions

S.-H. Suh et al.

Title Page

Abstract

Introduction

Conclusions

References

Tables

Figures

⏪

⏩

◀

▶

Back

Close

Full Screen / Esc

Printer-friendly Version

Interactive Discussion



quency of the PDF for convective rainfall was higher than that of stratiform rainfall when $\log_{10}(R) > 0.65 \text{ mm h}^{-1}$.

The PDF and CDF for horizontal reflectivity (Z_h), differential reflectivity (Z_{dr}), specific differential phase (K_{dp}), and specific attenuation of horizontal reflectivity (A_h) are shown in Fig. 4f–i. The PDF of Z_h for stratiform rainfall (Fig. 4f) is widely spread between 6 and 50 dBZ with the peak at approximately 30 dBZ. Conversely, for convective rainfall, frequencies lie between 25 and 55 dBZ and the peak frequency value at approximately 40 dBZ. The frequency value of reflectivity is higher for convective rainfall than for stratiform rainfall in the range of $\sim > 34 \text{ dBZ}$. Furthermore, the shape of the PDF for convective rainfall is similar to that reported for Darwin, Australia (Steiner et al., 1995); however, for stratiform rainfall there are significant differences between Busan and Darwin in terms of the shape of the frequency distribution. The method of classifying rainfall as convective when radar reflectivity is $> 38 \text{ dBZ}$, as proposed by Gamache and Houze Jr. (1982), is therefore not suitable in this instance because of the distribution of stratiform and convective rainfall types in Busan.

The PDF of Z_{dr} primarily exists between 0 and 2 dB, and the peaks are at 0.3 and 0.8 dB (Fig. 4g). The distribution of Z_{dr} for convective and stratiform rainfall is concentrated between 0.5 and 1.4 dB, and between 0.7 and 2 dB, respectively. The frequency of Z_{dr} for convective (stratiform) rainfall exists in ranges higher (lower) than 0.7 dB.

The dominant distribution of K_{dp} for the entire dataset and for stratiform rainfall lies between 0 and 0.14 deg km^{-1} , with a peak value of $5.0 \times 10^{-3} \text{ deg km}^{-1}$. However, for convective rainfall the PDF of K_{dp} is evenly spread between 0.01 and 0.15 deg km^{-1} . Furthermore, when $K_{dp} > 5.0 \times 10^{-2} \text{ deg km}^{-1}$, the frequency of the PDF for convective rainfall is higher than that of stratiform rainfall (Fig. 4h).

The PDF of A_h is similar to that of K_{dp} and is spread between 0 and $1.0 \times 10^{-2} \text{ dB km}^{-1}$. For the case of the entire rainfall dataset and for stratiform rainfall, the PDF of A_h is concentrated between 0 and $2.0 \times 10^{-3} \text{ dB km}^{-1}$ and that of convective rainfall is strongly concentrated between 1.0×10^{-3} and $8.0 \times 10^{-3} \text{ dB km}^{-1}$ (Fig. 4i). Unlike

Climatological characteristics of raindrop size distributions

S.-H. Suh et al.

Title Page

Abstract

Introduction

Conclusions

References

Tables

Figures

⏪

⏩

◀

▶

Back

Close

Full Screen / Esc

Printer-friendly Version

Interactive Discussion



The D_m (N_w) value for the typhoon category was considerably smaller (larger) than that of the other categories. This result does not agree with that reported by Chang et al. (2009), who noted that the D_m of convective rainfall typhoon showed a large value compared with that associated with stratiform rainfall.

3.3 Diurnal variation in raindrop size distributions

3.3.1 Diurnal variations in DSDs

Figure 7a shows a histogram of normalized frequency of 16 wind directions recorded by the AWS, which is the same instrument as that used to collect the data shown in Fig. 3. To establish the existence of a land–sea breeze, the difference in wind direction frequencies between DT and NT were analyzed. Figure 7b shows the difference between DT and NT in terms of the normalized frequency of 16 wind directions. Positive (negative) values indicate that the frequency of wind is higher in the DT (NT). The frequency of wind direction in the DT (NT), between 205.5° (22.5°) and 22.5° (205.5°), is higher than that in the NT (DT) (Fig. 7b). The observation site where the POSS was installed is located 611 m from the coast line, suggesting that the effect of the land–sea breeze would have been recorded. To understand the effects of the land–sea breeze on DSD characteristics, we analyzed the PDF and 2 h averaged DSD parameters for DT and NT. Figure 8 illustrates the distributions of μ , D_m , $\log_{10}(N_w)$, $\log_{10}(\text{LWC})$, $\log_{10}(R)$, and Z_h . There were large variations of μ with time. The μ values varied from 2.628 to 3.366 and the minimum and maximum μ values occurred at 08:00 KST and 22:00 KST, respectively (Fig. 8a). A D_m larger than 1.3 mm dominated from 00:00 KST to 12:00 KST, before decreasing dramatically between 12:00 and 14:00 KST. The minimum and maximum D_m appeared at 14:00 KST and 08:00 KST, respectively (Fig. 8b).

N_w generally varies inversely to D_m ; however, no inverse relationship was identified between D_m and N_w in our study (Fig. 8c). The maximum and minimum values of N_w were found at 06:00 KST and 22:00 KST.

Climatological characteristics of raindrop size distributions

S.-H. Suh et al.

[Title Page](#)

[Abstract](#)

[Introduction](#)

[Conclusions](#)

[References](#)

[Tables](#)

[Figures](#)

[⏪](#)

[⏩](#)

[◀](#)

[▶](#)

[Back](#)

[Close](#)

[Full Screen / Esc](#)

[Printer-friendly Version](#)

[Interactive Discussion](#)



Variability through time was similar for R , LWC, and Z_h . There was an increasing trend from 00:00 KST to 08:00 KST followed by a dramatically decreasing trend from 08:00 KST to 14:00 KST (Figs. 8d, 11e and f). Note that the time of the sharp decline for R between 12:00 KST and 14:00 KST is simultaneous with a D_m decrease. Larger (smaller) drops would contribute to higher R in the morning (afternoon).

The PDF distribution of μ between -2 and 0 is more concentrated for NT than for DT. Furthermore, when $\mu > 0$, DT and NT frequency distributions are similar (Fig. 9a). A larger number of smaller and larger raindrops would be expected in NT than in DT.

The distribution of DT $D_m < 0.7$ mm is wider than that of the NT. However, between 0.7 and 1.5 mm the frequency for NT is higher than that for DT, whereas the distribution in the range > 1.5 mm is similar for both DT and NT (Fig. 9b). We note that the smaller peak of D_m around 0.6 mm for the entire rainfall dataset (Fig. 4b) was observed only in DT.

The distribution of $\log_{10}(N_w)$ for DT (NT) is narrower than that of NT (DT) between 4 and $5.2 \text{ m}^{-3} \text{ mm}^{-1}$ (2.8 and $4 \text{ m}^{-3} \text{ mm}^{-1}$) (Fig. 9c).

Bringi et al. (2003) noted that the maritime climatology displayed larger N_w and smaller D_m values than the continental climatology, based on observed DSDs in the low and middle latitude. Also, Göke et al. (2007) emphasized that rainfall type can be defined by the origin location and movement direction. In accordance with these previous results, we consider NT rainfall in the Busan region to be more likely caused by a continental convective system.

Kozu et al. (2006) analyzed the diurnal variation in R at Gadanki (South India), Singapore, and Kototabang (West Sumatra) during the summer monsoon season. All regions displayed maximum R at approximately 16:00 KST, except for Gadanki. Qian (2008) also examined the diurnal variation of accumulated rain amount on Java Island, Indonesia, for 30 years from 1971 to 2000. Rainfall occurred mainly on land areas (over the ocean) in the DT (NT) when the sea (land) breeze was dominant.

In the present study, the shape of the PDF of LWC and R for DT and NT are similar. LWC and R distributions during the DT (NT) are higher (lower) than in the NT (DT)

when LWC and R are smaller (greater) than $6.3 \times 10^{-3} \text{ g m}^{-3}$ and 1 mm h^{-1} , respectively (Fig. 9d and e). The positive relationship between horizontal radar reflectivity and LWC and R during the DT (NT) was higher (lower) than in the NT (DT) in the range below (above) about 27 dBZ (Fig. 9f).

3.3.2 Diurnal variations of DSDs with respect to season

Busan experiences distinct atmospheric conditions that are caused by the different frequencies and magnitudes of land–sea breezes in response to variable sunrise and sunset times. To identify seasonal variations of DSDs with respect to the effect of the land–sea breeze, we analyzed the DT and NT PDF of D_m and N_w in the summer and winter. The start and end times of DT (NT) were sorted using the latest sunrise (sunset) and the earliest sunset (sunrise) time for each season (Table 4).

Figure 10 shows a histogram of wind directions in summer and winter for the entire period. The frequencies of summer and winter wind directions are similar to each other. However, in Fig. 11, the DT and NT distributions of winter wind direction display opposing frequencies between 0 and 45°, which is a land and ocean area, and between 90 and 225°, which is an ocean area. In other words, in contrast to the summer, the frequency of land breeze increased (decreased) during the DT (NT) in winter.

To identify the variability of DSDs caused by the land–sea breeze in summer and winter, a 2 h interval time series of D_m , N_w and R was analyzed. In the summer, the time series of D_m displays considerably large values between 00:00 KST and 12:00 KST, compared with the period between 14:00 KST and 22:00 KST (Fig. 12a). The mean value of D_m decreases dramatically between 12:00 KST and 14:00 KST. N_w generally has a negative relationship with D_m , except at 18:00 KST and 20:00 KST (Fig. 12b). A time series of D_m for the Busan area shows a relatively large value from 00:00 KST to 12:00 KST and a relatively small value from 14:00 KST to 22:00 KST. In the case of N_w , however, the value was relatively small from 00:00 KST to 12:00 KST and there was no clear pattern for larger values. There are two peaks of $\log_{10}(N_w)$, at 06:00 KST and

Title Page

Abstract

Introduction

Conclusions

References

Tables

Figures



Back

Close

Full Screen / Esc

Printer-friendly Version

Interactive Discussion



Climatological characteristics of raindrop size distributions

S.-H. Suh et al.

Title Page

Abstract

Introduction

Conclusions

References

Tables

Figures

⏪

⏩

◀

▶

Back

Close

Full Screen / Esc

Printer-friendly Version

Interactive Discussion



20:00 KST (Fig. 12b). The rainfall rate tends to increase gradually from 00:00 KST to 08:00 KST and decrease from 08:00 KST to 14:00 KST, which is similar to the pattern of R (Fig. 12c). The D_m time series is similar to results from Qian (2008), who analyzed the diurnal variability of wind direction and R on Java Island during the summer season using 30 years (from 1971 to 2000) of NCEP/NCAR reanalyzed data. They found that a land-breeze occurred from 01:00 KST to 10:00 KST and a sea-breeze from 13:00 KST to 22:00 KST (Fig. 7 of Qian, 2008).

Variability of the winter D_m time series is the inverse of the summer time series (Fig. 13a). The mean value of D_m steadily increases from 00:00 KST to 16:00 KST and then decreases from 16:00 KST to 22:00 KST. The winter N_w time series displays a clear inverse pattern compared with the D_m variation with time (Fig. 13b). The mean value of $\log_{10}(N_w)$ increases from 16:00 KST to 04:00 KST and then steadily decreases from 04:00 KST to 16:00 KST. The peak occurs at 04:00 KST (Fig. 13c).

The PDF distribution of summer D_m displays a relatively large DT frequency compared with NT when $D_m < 1.65$ mm, except for the range between 0.7 and 1 mm. However, in the range of $D_m > 1.65$ mm, the NT PDF displays a larger frequency (Fig. 14a). The PDF of $\log_{10}(N_w)$ for NT has a larger frequency than the DT when $\log_{10}(N_w) < 3.3 \text{ m}^{-3} \text{ mm}^{-1}$ but smaller frequency when $\log_{10}(N_w) > 3.3 \text{ m}^{-3} \text{ mm}^{-1}$ (Fig. 14b).

The DT and NT PDFs of D_m and $\log_{10}(N_w)$ during winter display an inverse distribution. For the PDF of D_m , there is a considerable frequency for NT (DT) when $D_m < (>)$ 1.6 mm (Fig. 15a). The PDF of $\log_{10}(N_w)$ during summer display an inverse distribution to that of the winter. The PDF frequency of summer season for NT (DT) is larger than that of the DT(NT) when $\log_{10}(N_w) < (>)$ $3.3 \text{ m}^{-3} \text{ mm}^{-1}$ (Fig. 14b). However, during the winter DT (NT) a relatively large frequency exists when $\log_{10}(N_w) < (>)$ $3.5 \text{ m}^{-3} \text{ mm}^{-1}$ (Fig. 15b). Relatively large (small) D_m and small (large) $\log_{10}(N_w)$ are displayed during the NT (DT) when a land-breeze (sea-breeze) occurs.

4 Summary and conclusion

Climatological characteristics of DSDs in Busan were analyzed using the DSD data observed by POSS over a four-year period from 24 February 2001 to 24 December 2004. Observed DSDs were filtered to remove error by performing several quality control measures, and an AWS rain gauge installed nearby was used to verify the rainfall amount recorded by the POSS. We analyzed DSD characteristics of convective and stratiform rainfall types, as defined by Bringi et al. (2003). The rainfall dataset was thus divided into stratiform and convective rainfall and their contributions to the total rainfall were 90.6 and 5.8 %, respectively.

In the comparison of DSD parameters observed between Busan and Järvenpää, the averaged rainfall rate in Busan was higher than in Järvenpää. D_0 was smaller and N_w larger in Busan compared with Järvenpää and there was a considerable difference in μ between the two cities. We consider that the greater number of smaller drops contributes to the higher rainfall rate in the mid latitudes. According to the study by Bringi et al. (2003), the rainfall in Busan has more maritime climatological DSD characteristics.

The mean values of D_m and N_w for stratiform rainfall are relatively small compared with the average line of stratiform rainfall produced by Bringi et al. (2003), except for heavy rainfall events. The mean values of D_m and N_w for convective type for all rainfall categories converged around the maritime cluster, except for the typhoon category. The convective rainfall associated with a typhoon has considerably smaller D_m and larger N_w values compared with the other rainfall categories. This is likely caused by increased raindrop break-up as a result of strong wind effects. Furthermore, the distributions of mean D_m and N_w values for all rainfall categories associated with convective rainfall display a linear relationship, apart from the typhoon category.

The analysis of diurnal variation in DSD yielded the following results: first, in the negative range of μ , the frequency of μ is higher at night than during the DT. The PDF of R is higher at NT than during the DT when $\log_{10}(R) > 0.6 \text{ mm h}^{-1}$. A gentle

HESSD

12, 4005–4045, 2015

Climatological characteristics of raindrop size distributions

S.-H. Suh et al.

Title Page

Abstract

Introduction

Conclusions

References

Tables

Figures

⏪

⏩

◀

▶

Back

Close

Full Screen / Esc

Printer-friendly Version

Interactive Discussion



Climatological characteristics of raindrop size distributions

S.-H. Suh et al.

[Title Page](#)

[Abstract](#)

[Introduction](#)

[Conclusions](#)

[References](#)

[Tables](#)

[Figures](#)

[⏪](#)

[⏩](#)

[◀](#)

[▶](#)

[Back](#)

[Close](#)

[Full Screen / Esc](#)

[Printer-friendly Version](#)

[Interactive Discussion](#)



peak of D_m was identified during the DT at approximately 0.6 mm for both stratiform and convective rainfall. Additionally, the frequency of D_m is higher at NT than during the DT when $D_m > 0.65 \text{ mm h}^{-1}$. For N_w , which tends to be inversely related to D_m , its frequency is higher at NT than during the DT when $\log_{10}(N_w) > 3.9 \text{ m}^{-3} \text{ mm}^{-1}$. At NT, D_m is higher and R , μ , and N_w values are lower compared with the DT. In other words, maritime characteristics are observed in the DT more often than in the NT, based on the results of Bringi et al. (2003). The above-mentioned DSD characteristics are likely due to the land–sea breeze caused by differences in specific heat between the land and ocean. These features are also apparent in the seasonal diurnal distribution. The PDF of DT and NT during the summer is similar to the PDF of the entire period; however, the PDF of DT and NT in the winter displays the inverse distribution because of seasonal differences in wind direction.

Author contributions. C.-H. You designed the study. S.-H. Suh modified the original study theme and performed the study. C.-H. You and S.-H. Suh *performed research*, obtained the results and prepared the manuscript along with contributions from all of the co-authors. D.-I. Lee examined the results and checked the manuscript.

Acknowledgements. This research was supported by the National Research Foundation of Korea (NRF) through a grant provided by the Korean Ministry of Education, Science & Technology (MEST) in 2015 (No. 200603874) and the Korea Meteorological Administration Research and Development Program under Grant CATER 2012-2071.

References

- Andsager, K., Beard, K. V., and Laird, N. F.: Laboratory measurements of axis ratios for large raindrops, *J. Atmos. Sci.*, 56, 2673–2683, 1999.
- Atlas, D., Srivastava, R., and Sekhon, R. S.: Doppler radar characteristics of precipitation at vertical incidence, *Rev. Geophys.*, 11, 1–35, 1973.
- Atlas, D., Ulbrich, C. W., Marks, F. D., Amitai, E., and Williams, C. R.: Systematic variation of drop size and radar-rainfall relations, *J. Geophys. Res.-Atmos.*, 104, 6155–6169, 1999.

Climatological characteristics of raindrop size distributions

S.-H. Suh et al.

[Title Page](#)

[Abstract](#)

[Introduction](#)

[Conclusions](#)

[References](#)

[Tables](#)

[Figures](#)

[⏪](#)

[⏩](#)

[◀](#)

[▶](#)

[Back](#)

[Close](#)

[Full Screen / Esc](#)

[Printer-friendly Version](#)

[Interactive Discussion](#)



- Beard, K. V. and Chuang, C.: A new model for the equilibrium shape of raindrops, *J. Atmos. Sci.*, 44, 1509–1524, 1987.
- Brandes, E. A., Zhang, G., and Vivekanandan, J.: Experiments in rainfall estimation with a polarimetric radar in a subtropical environment, *J. Appl. Meteorol.*, 41, 674–685, 2002.
- 5 Bringi, V., Chandrasekar, V., Hubbert, J., Gorgucci, E., Randeu, W., and Schoenhuber, M.: Raindrop size distribution in different climatic regimes from disdrometer and dual-polarized radar analysis, *J. Atmos. Sci.*, 60, 354–365, 2003.
- Chang, W.-Y., Wang, T.-C. C., and Lin, P.-L.: Characteristics of the raindrop size distribution and drop shape relation in typhoon systems in the western Pacific from the 2D video disdrometer and NCU C-band polarimetric radar, *J. Atmos. Ocean. Tech.*, 26, 1973–1993, 2009.
- 10 Dou, X., Testud, J., Amayenc, P., and Black, R.: The parameterization of rain for a weather radar, *C.R. Acad. Sci. II A*, 328, 577–582, 1999.
- Feingold, G. and Levin, Z.: The lognormal fit to raindrop spectra from frontal convective clouds in Israel, *J. Clim. Appl. Meteorol.*, 25, 1346–1363, 1986.
- 15 Gamache, J. F. and Houze Jr., R. A.: Mesoscale air motions associated with a tropical squall line, *Mon. Weather Rev.*, 110, 118–135, 1982.
- Göke, S., Ochs III, H. T., and Rauber, R. M.: Radar analysis of precipitation initiation in maritime versus continental clouds near the Florida coast: inferences concerning the role of CCN and giant nuclei, *J. Atmos. Sci.*, 64, 3695–3707, 2007.
- 20 Gunn, R. and Kinzer, G. D.: The terminal velocity of fall for water droplets in stagnant air, *J. Meteorol.*, 6, 243–248, 1949.
- Hu, Z. and Srivastava, R.: Evolution of raindrop size distribution by coalescence, breakup, and evaporation: theory and observations, *J. Atmos. Sci.*, 52, 1761–1783, 1995.
- Johnson, R. H. and Hamilton, P. J.: The relationship of surface pressure features to the precipitation and airflow structure of an intense midlatitude squall line, *Mon. Weather Rev.*, 116, 1444–1473, 1988.
- 25 Kozu, T., Reddy, K. K., Mori, S., Thurai, M., Ong, J. T., Rao, D. N., and Shimomai, T.: Seasonal and diurnal variations of raindrop size distribution in Asian monsoon region, *J. Meteorol. Soc. Jpn.*, 84, 195–209, 2006.
- 30 Leinonen, J., Moisseev, D., Leskinen, M., and Petersen, W. A.: A climatology of disdrometer measurements of rainfall in Finland over five years with implications for global radar observations, *J. Appl. Meteorol. Clim.*, 51, 392–404, 2012.

Climatological characteristics of raindrop size distributions

S.-H. Suh et al.

[Title Page](#)

[Abstract](#)

[Introduction](#)

[Conclusions](#)

[References](#)

[Tables](#)

[Figures](#)

[⏪](#)

[⏩](#)

[◀](#)

[▶](#)

[Back](#)

[Close](#)

[Full Screen / Esc](#)

[Printer-friendly Version](#)

[Interactive Discussion](#)



- Levin, Z.: Charge separation by splashing of naturally falling raindrops, *J. Atmos. Sci.*, 28, 543–548, 1971.
- Mapes, B. E. and Houze Jr., R. A.: Cloud clusters and superclusters over the oceanic warm pool, *Mon. Weather Rev.*, 121, 1398–1416, 1993.
- 5 Markowitz, A. H.: Raindrop size distribution expressions, *J. Appl. Meteorol.*, 15, 1029–1031, 1976.
- Marshall, J. S. and Palmer, W. M. K.: The distribution of raindrops with size, *J. Meteorol.*, 5, 165–166, 1948.
- Mueller, E. A.: Radar Cross Sections from Drop Size Spectra, University of Illinois, Urbana-Champaign, 1966.
- 10 Pruppacher, H. and Beard, K.: A wind tunnel investigation of the internal circulation and shape of water drops falling at terminal velocity in air, *Q. J. Roy. Meteor. Soc.*, 96, 247–256, 1970.
- Qian, J.-H.: Why precipitation is mostly concentrated over islands in the Maritime Continent, *J. Atmos. Sci.*, 65, 1428–1441, 2008.
- 15 Ray, P. S.: Broadband complex refractive indices of ice and water, *Appl. Optics*, 11, 1836–1844, 1972.
- Sauvageot, H. and Lacaux, J.-P.: The shape of averaged drop size distributions, *J. Atmos. Sci.*, 52, 1070–1083, 1995.
- Seliga, T. and Bringi, V.: Potential use of radar differential reflectivity measurements at orthogonal polarizations for measuring precipitation, *J. Appl. Meteorol.*, 15, 69–76, 1976.
- 20 Sheppard, B. and Joe, P.: Performance of the precipitation occurrence sensor system as a precipitation gauge, *J. Atmos. Ocean. Tech.*, 25, 196–212, 2008.
- Steiner, M., Houze Jr., R. A., and Yuter, S. E.: Climatological characterization of three-dimensional storm structure from operational radar and rain gauge data, *J. Appl. Meteorol.*, 34, 1978–2007, 1995.
- 25 Testud, J., Oury, S., Black, R. A., Amayenc, P., and Dou, X.: The concept of “normalized” distribution to describe raindrop spectra: a tool for cloud physics and cloud remote sensing, *J. Appl. Meteorol.*, 40, 1118–1140, 2001.
- Tokay, A. and Short, D. A.: Evidence from tropical raindrop spectra of the origin of rain from stratiform versus convective clouds, *J. Appl. Meteorol.*, 35, 355–371, 1996.
- 30 Ulbrich, C. W.: Natural variations in the analytical form of the raindrop size distribution, *J. Clim. Appl. Meteorol.*, 22, 1764–1775, 1983.

- Ulbrich, C. W. and Atlas, D.: Rainfall microphysics and radar properties: analysis methods for drop size spectra, *J. Appl. Meteorol.*, 37, 912–923, 1998.
- Waldvogel, A.: The N₀ jump of raindrop spectra, *J. Atmos. Sci.*, 31, 1067–1078, 1974.
- Waterman, P.: Symmetry, unitarity, and geometry in electromagnetic scattering, *Phys. Rev. D*, 3, 825–839, 1971.
- Willis, P. T.: Functional fits to some observed drop size distributions and parameterization of rain, *J. Atmos. Sci.*, 41, 1648–1661, 1984.
- You, C.-H., Lee, D.-I., and Kang, M.-Y.: Rainfall estimation using specific differential phase for the first operational polarimetric radar in Korea, *Adv. Meteorol.*, 2014, 413717, doi:10.1155/2014/413717, 2014.
- Zhang, G., Vivekanandan, J., and Brandes, E.: A method for estimating rain rate and drop size distribution from polarimetric radar measurements, *IEEE T. Geosci. Remote*, 39, 830–841, 2001.

HESSD

12, 4005–4045, 2015

Climatological characteristics of raindrop size distributions

S.-H. Suh et al.

Title Page

Abstract

Introduction

Conclusions

References

Tables

Figures

⏪

⏩

◀

▶

Back

Close

Full Screen / Esc

Printer-friendly Version

Interactive Discussion



HESSD

12, 4005–4045, 2015

Climatological characteristics of raindrop size distributions

S.-H. Suh et al.

[Title Page](#)

[Abstract](#)

[Introduction](#)

[Conclusions](#)

[References](#)

[Tables](#)

[Figures](#)



[Back](#)

[Close](#)

[Full Screen / Esc](#)

[Printer-friendly Version](#)

[Interactive Discussion](#)



Table 2. Mean value of DSDs for Busan and Järvenpää.

Parameter	Järvenpää, Finland	Busan, Korea
$\bar{\mu}$	8.80	3.04
D_0	1.34	1.27
$\log_{10}(\overline{N_w})$	3.69	4.40
$\log_{10}(\overline{R})$	0.13	0.39

Climatological characteristics of raindrop size distributions

S.-H. Suh et al.

Table 3. Rainfall rate for each rainfall category and the number of sample size for 1 min data.

Rainfall Category	Entire rainfall	Stratiform rainfall (%)	Convective rainfall (%)
Typhoon	5658	4629 (81.81)	700 (12.37)
Changma	22 308	19 238 (86.23)	1849 (8.28)
Heavy rainfall	381	219 (57.48)	118 (30.97)
Spring	34 427	31 831 (92.45)	1545 (4.48)
Summer	43 174	37 054 (85.82)	3750 (8.65)
Autumn	22 717	21 383 (94.12)	806 (3.54)
Winter	13 837	13 161 (95.11)	386 (2.78)
Daytime	47 357	42 937 (90.66)	2682 (5.66)
Nighttime	43 444	39 473 (90.85)	2389 (5.49)
Entire	114 155	103 429 (90.60)	6487 (5.68)

[Title Page](#)
[Abstract](#)
[Introduction](#)
[Conclusions](#)
[References](#)
[Tables](#)
[Figures](#)
[⏪](#)
[⏩](#)
[◀](#)
[▶](#)
[Back](#)
[Close](#)
[Full Screen / Esc](#)
[Printer-friendly Version](#)
[Interactive Discussion](#)


HESSD

12, 4005–4045, 2015

Climatological characteristics of raindrop size distributions

S.-H. Suh et al.

[Title Page](#)[Abstract](#)[Introduction](#)[Conclusions](#)[References](#)[Tables](#)[Figures](#)[Back](#)[Close](#)[Full Screen / Esc](#)[Printer-friendly Version](#)[Interactive Discussion](#)**Table 4.** DT and NT (KST) in summer and winter season.

Rainfall Category	Type	Beginning time (KST)	Finishing time (KST)
Summer	DT	05:33	19:27
	NT	19:42	05:09
Winter	DT	07:33	17:12
	NT	18:19	06:54



Figure 1. Photograph of the POSS instrument used in this research.

HESSD

12, 4005–4045, 2015

Climatological characteristics of raindrop size distributions

S.-H. Suh et al.

[Title Page](#)

[Abstract](#)

[Introduction](#)

[Conclusions](#)

[References](#)

[Tables](#)

[Figures](#)

[◀](#)

[▶](#)

[◀](#)

[▶](#)

[Back](#)

[Close](#)

[Full Screen / Esc](#)

[Printer-friendly Version](#)

[Interactive Discussion](#)



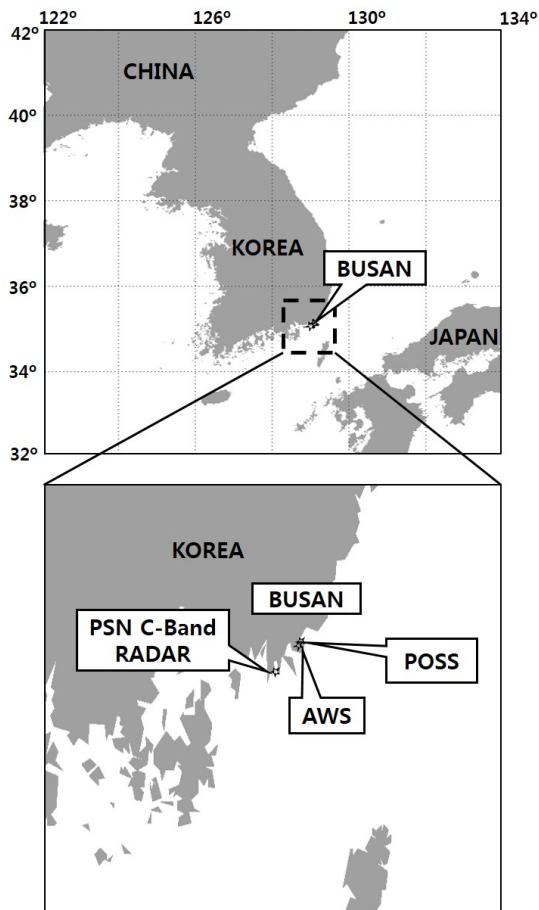


Figure 2. Locations of the POSS and the AWS rain gauge installed in Busan, Korea.

HESSD

12, 4005–4045, 2015

Climatological characteristics of raindrop size distributions

S.-H. Suh et al.

Title Page	
Abstract	Introduction
Conclusions	References
Tables	Figures
◀	▶
◀	▶
Back	Close
Full Screen / Esc	
Printer-friendly Version	
Interactive Discussion	



Climatological characteristics of raindrop size distributions

S.-H. Suh et al.

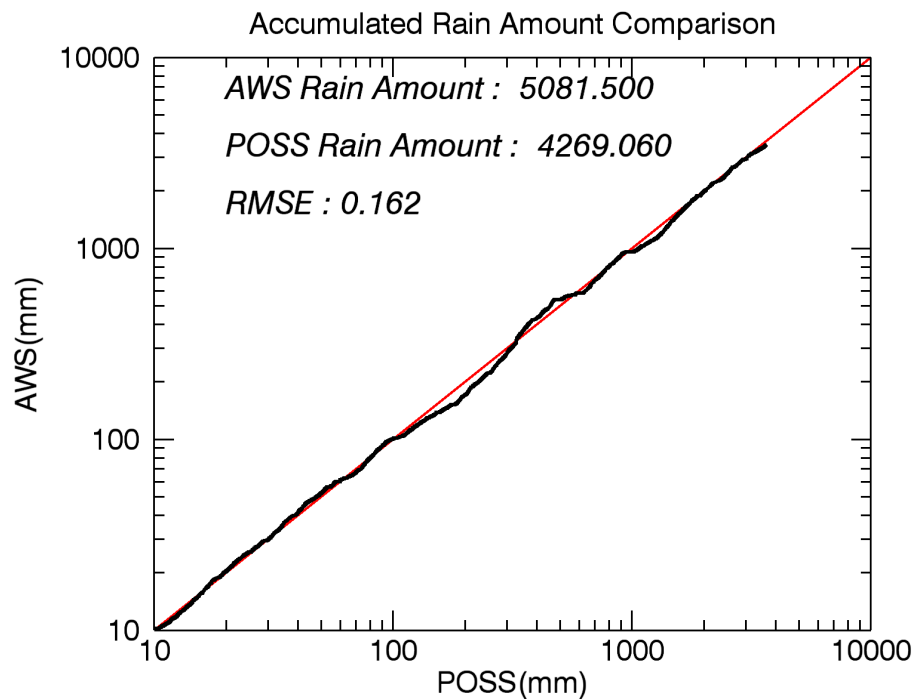


Figure 3. Comparison of the recorded rainfall amounts between the POSS and AWS instruments.

[Title Page](#)[Abstract](#)[Introduction](#)[Conclusions](#)[References](#)[Tables](#)[Figures](#)[⏪](#)[⏩](#)[◀](#)[▶](#)[Back](#)[Close](#)[Full Screen / Esc](#)[Printer-friendly Version](#)[Interactive Discussion](#)

Climatological characteristics of raindrop size distributions

S.-H. Suh et al.

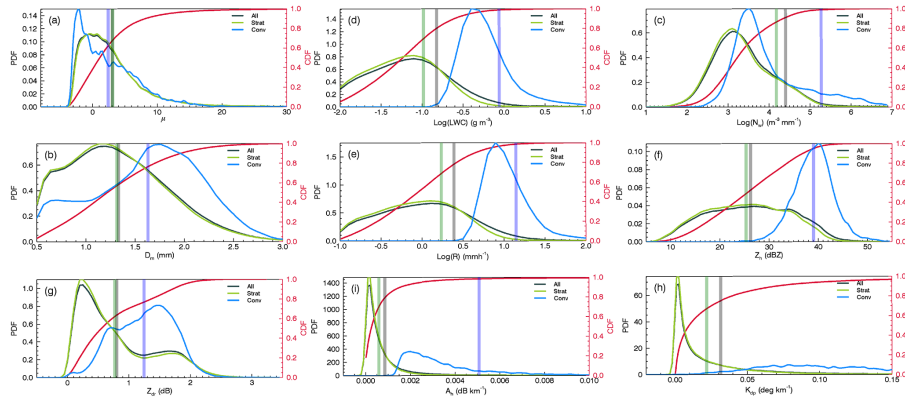


Figure 4. PDF and CDF curves for (a) μ , (b) D_m , (c) $\log_{10}(N_w)$, (d) $\log_{10}(R)$, (e) $\log_{10}(LWC)$, (f) Z_h , (g) Z_{dr} , (h) K_{dp} , and (i) A_h for the entire rainfall dataset (solid black line), stratiform rainfall (solid green line), and convective rainfall (solid blue line). The solid red line represents the CDF for entire rainfall dataset. The solid vertical line represents the mean value of each type.

Title Page

Abstract

Introduction

Conclusions

References

Tables

Figures

◀

▶

◀

▶

Back

Close

Full Screen / Esc

Printer-friendly Version

Interactive Discussion



Climatological characteristics of raindrop size distributions

S.-H. Suh et al.

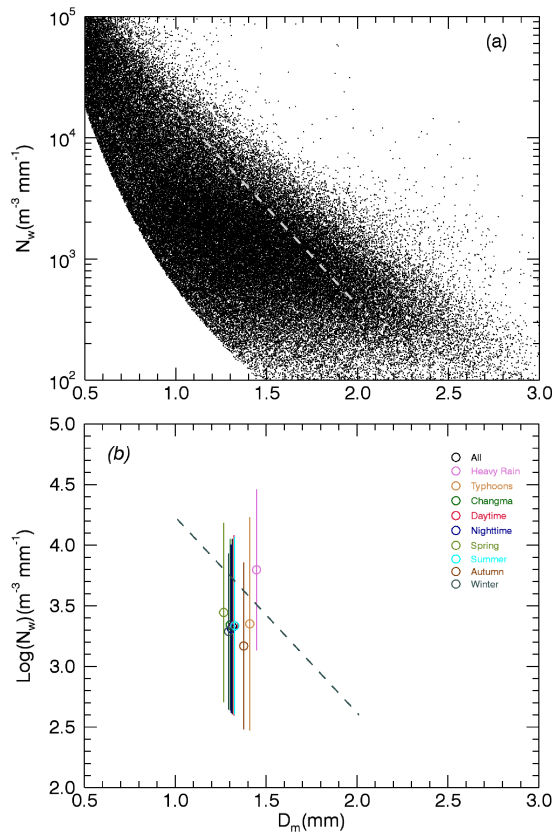


Figure 5. (a) Scatter plot of 1 min D_m and N_w for the 10 rainfall categories with respect to stratiform rainfall data. The broken grey line represents the average line, as defined by Bringi et al. (2003). (b) Scatter plot of mean D_m and $\log_{10}(N_w)$ values of the 10 rainfall categories with respect to stratiform rainfall. The vertical line represents $\pm 1\sigma$ for each category.

Climatological characteristics of raindrop size distributions

S.-H. Suh et al.

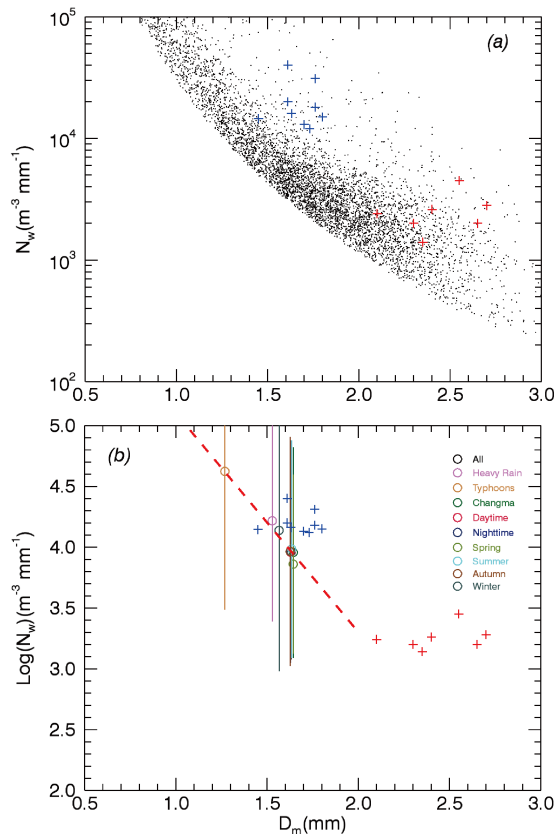


Figure 6. (a) As in Fig. 5a, but for convective rainfall. The blue and red symbols represent maritime and continental rainfall, respectively, as defined by Bringi et al. (2003). (b) As in Fig. 5b, but for convective rainfall. The broken red line represents the mathematical expression described in Eq. (15).

[Title Page](#)
[Abstract](#)
[Introduction](#)
[Conclusions](#)
[References](#)
[Tables](#)
[Figures](#)
[◀](#)
[▶](#)
[◀](#)
[▶](#)
[Back](#)
[Close](#)
[Full Screen / Esc](#)
[Printer-friendly Version](#)
[Interactive Discussion](#)


Climatological characteristics of raindrop size distributions

S.-H. Suh et al.

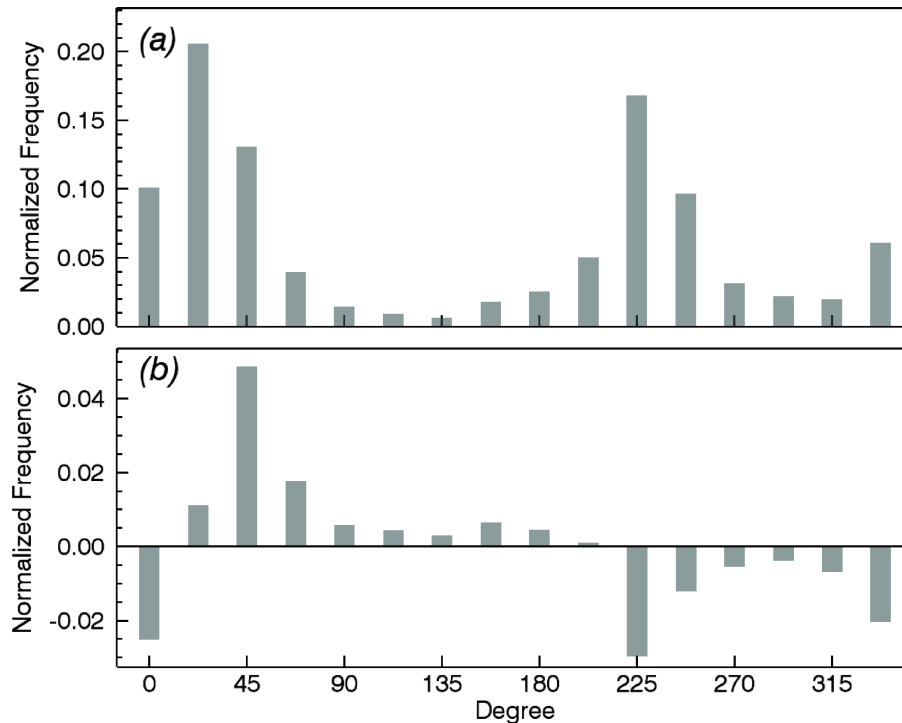


Figure 7. (a) Histogram of normalized frequency of 16 wind directions for the entire study period. (b) Difference in wind direction frequencies between DT and NT.

Climatological characteristics of raindrop size distributions

S.-H. Suh et al.

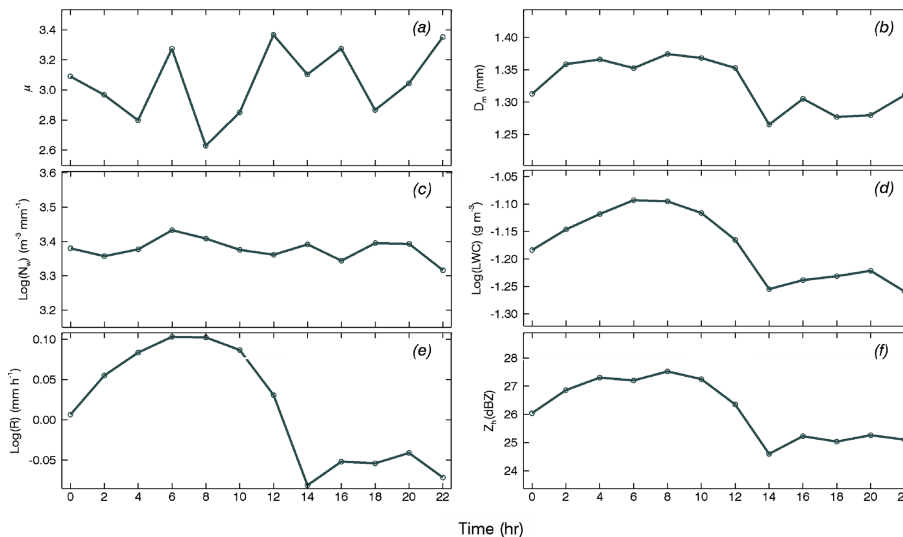


Figure 8. Time series of (a) μ , (b) D_m , (c) $\log_{10}(N_w)$, (d) $\log_{10}(R)$, (e) $\log_{10}(\text{LWC})$, and (f) Z_h collected for the total period.

[Title Page](#)
[Abstract](#)
[Introduction](#)
[Conclusions](#)
[References](#)
[Tables](#)
[Figures](#)
[⏪](#)
[⏩](#)
[◀](#)
[▶](#)
[Back](#)
[Close](#)
[Full Screen / Esc](#)
[Printer-friendly Version](#)
[Interactive Discussion](#)


Climatological characteristics of raindrop size distributions

S.-H. Suh et al.

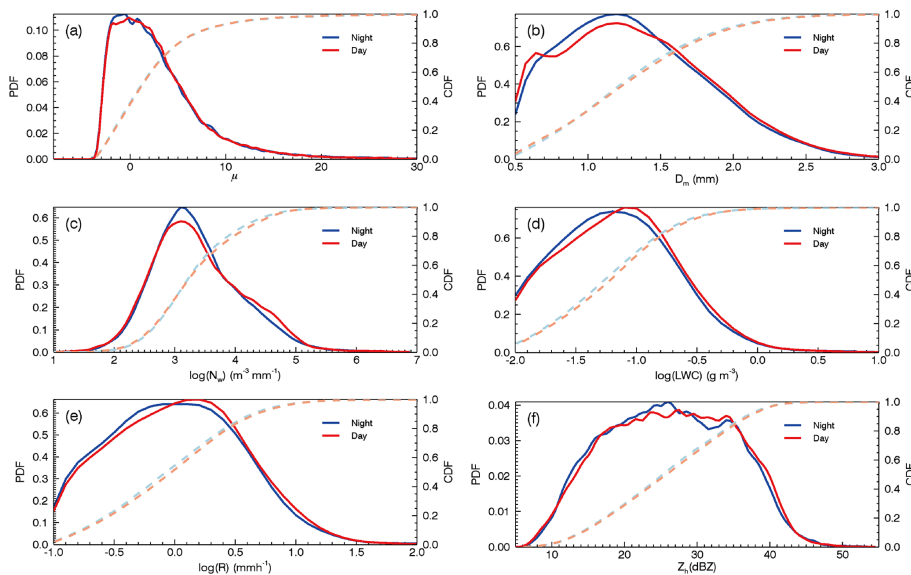


Figure 9. PDF and CDF curves for (a) μ , (b) D_m , (c) $\log_{10}(N_w)$, (d) $\log_{10}(R)$, (e) $\log_{10}(\text{LWC})$, and (f) Z_h for DT and NT. The solid red and blue lines represent the PDF for DT and NT, respectively. The broken light red and blue lines represent the CDF for DT and NT, respectively.

[Title Page](#)
[Abstract](#)
[Introduction](#)
[Conclusions](#)
[References](#)
[Tables](#)
[Figures](#)
[⏪](#)
[⏩](#)
[⏴](#)
[⏵](#)
[Back](#)
[Close](#)
[Full Screen / Esc](#)
[Printer-friendly Version](#)
[Interactive Discussion](#)


Climatological characteristics of raindrop size distributions

S.-H. Suh et al.

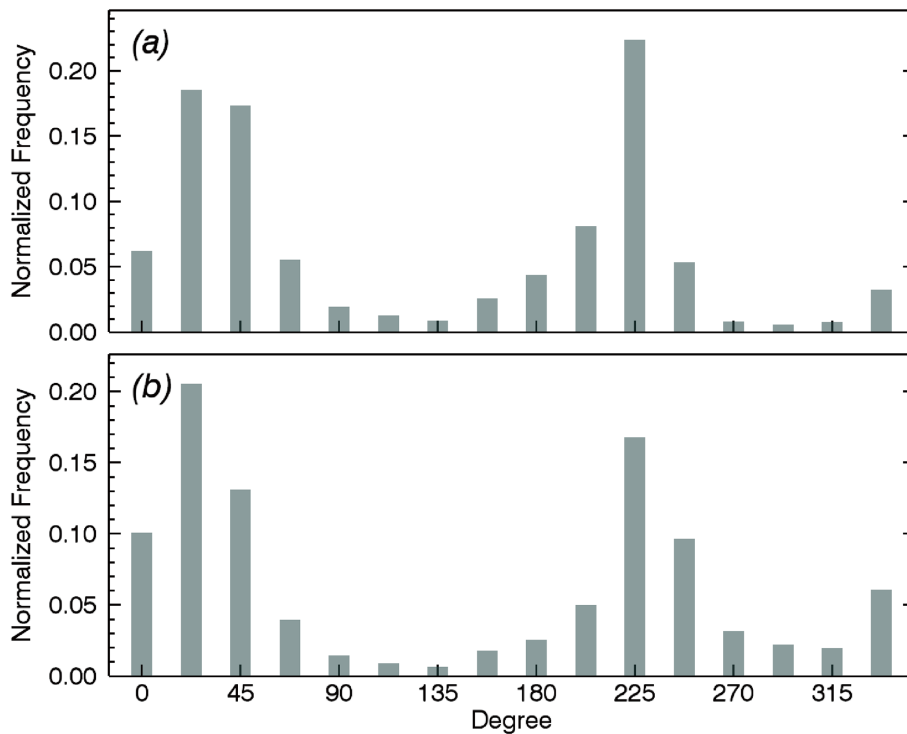


Figure 10. Histogram of normalized frequency for 16 wind directions in (a) summer and (b) winter.

Climatological characteristics of raindrop size distributions

S.-H. Suh et al.

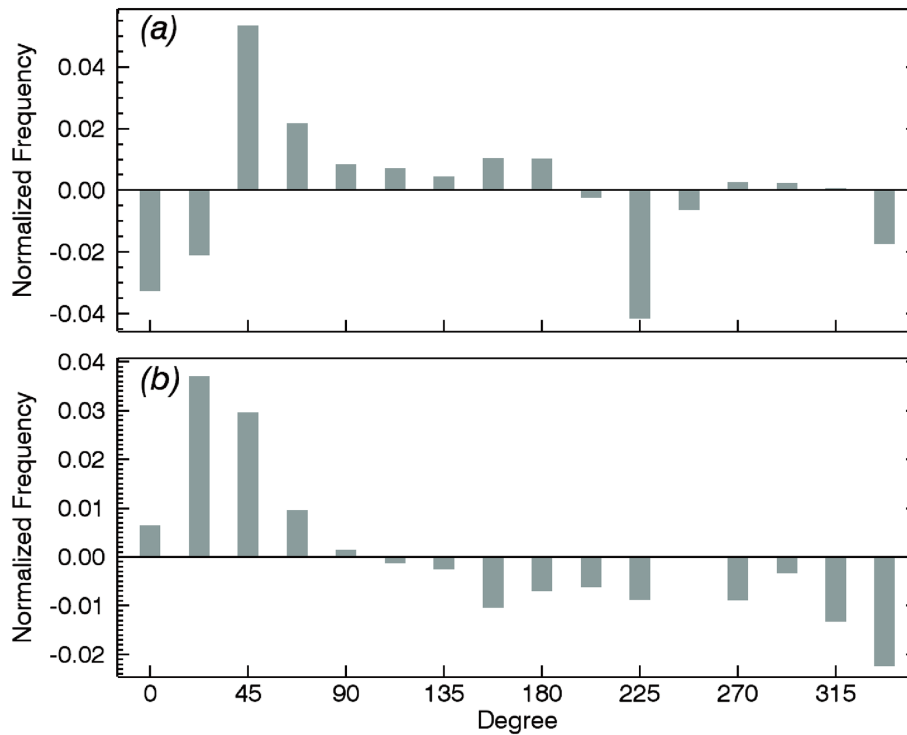


Figure 11. Histogram illustrating the difference in normalized frequency between DT and NT in (a) summer and (b) winter.

Climatological characteristics of raindrop size distributions

S.-H. Suh et al.

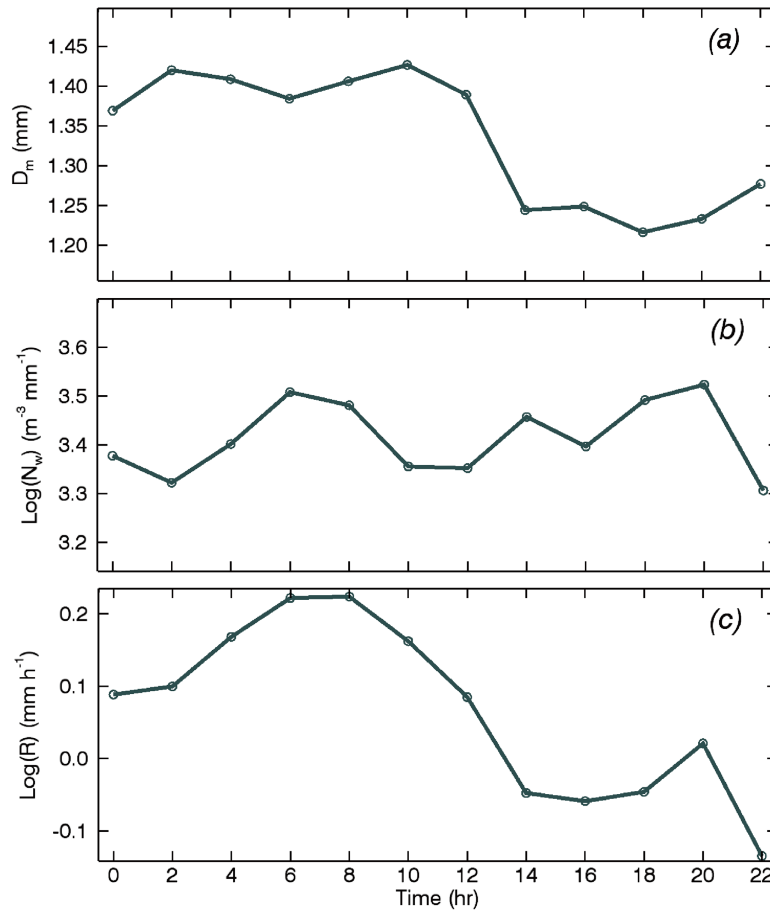


Figure 12. Time series of (a) D_m , (b) N_w , and (c) R for the summer.

Climatological characteristics of raindrop size distributions

S.-H. Suh et al.

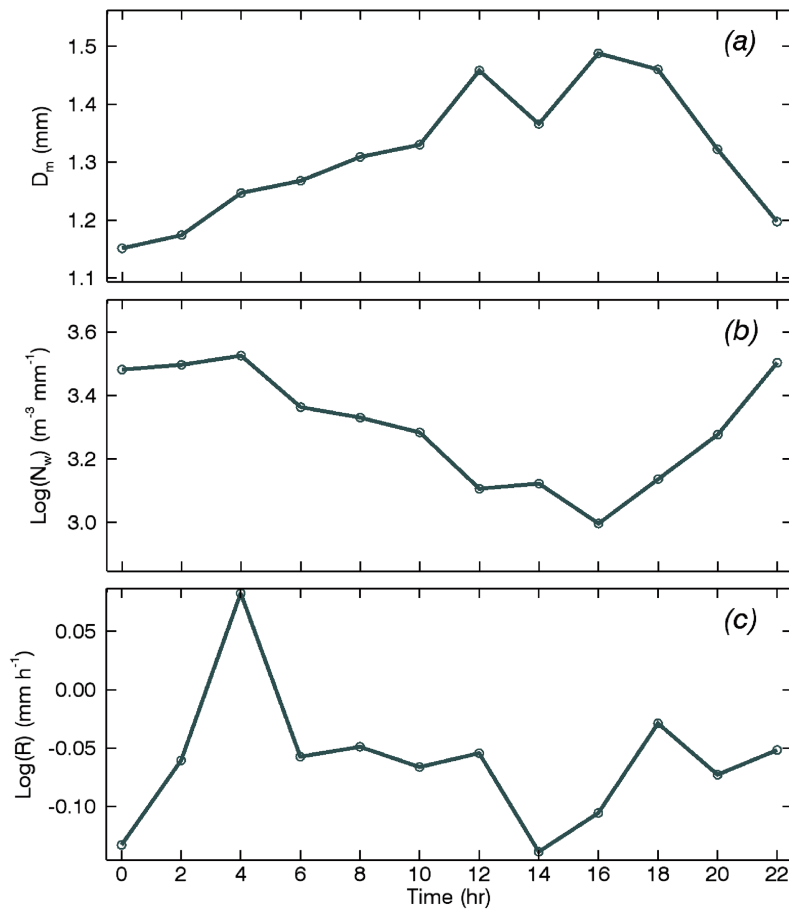


Figure 13. As in Fig. 12, but for winter.

Climatological characteristics of raindrop size distributions

S.-H. Suh et al.

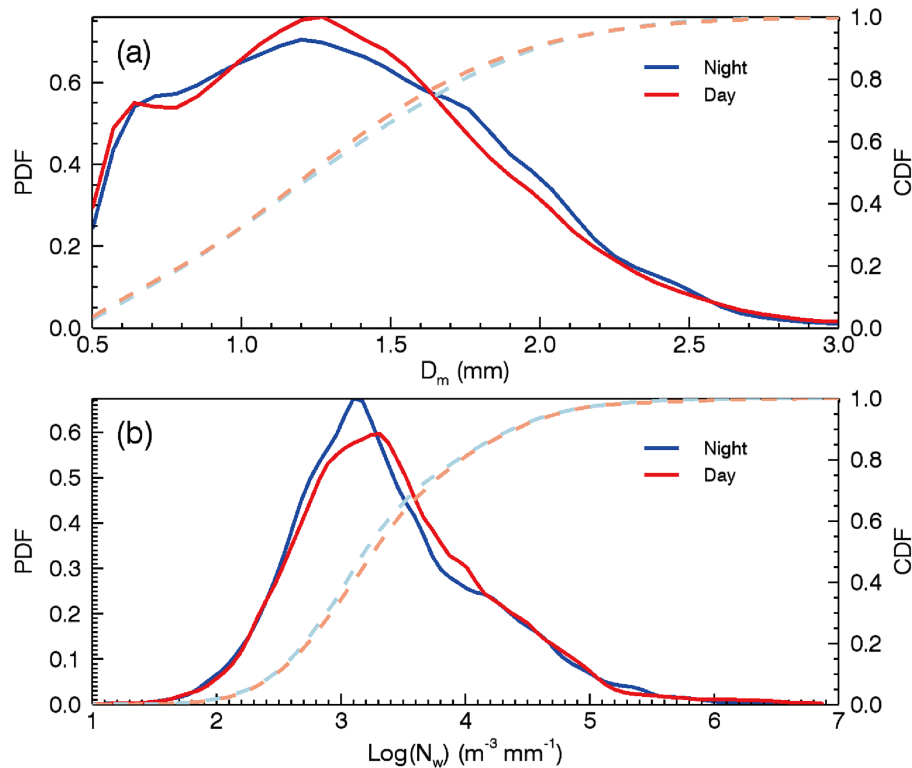
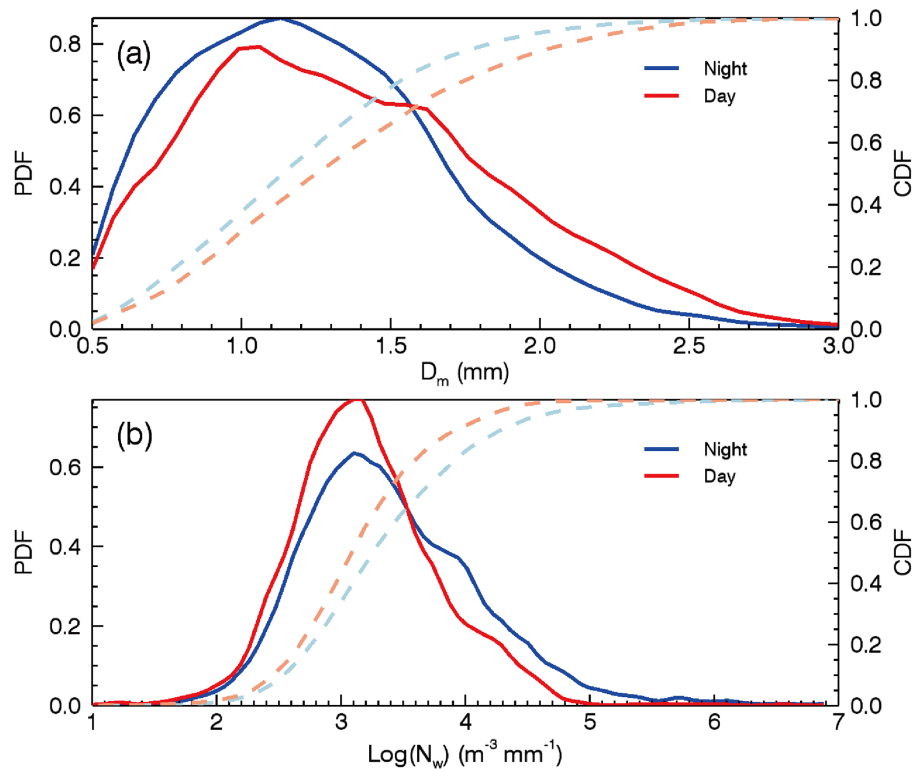


Figure 14. PDF and CDF of (a) DT and (b) NT in the summer. Red and blue solid lines represent the PDF of DT and NT, respectively. The light red and blue broken line represent the CDF for each season.

[Title Page](#)
[Abstract](#)
[Introduction](#)
[Conclusions](#)
[References](#)
[Tables](#)
[Figures](#)
[◀](#)
[▶](#)
[◀](#)
[▶](#)
[Back](#)
[Close](#)
[Full Screen / Esc](#)
[Printer-friendly Version](#)
[Interactive Discussion](#)


Climatological characteristics of raindrop size distributions

S.-H. Suh et al.

**Figure 15.** As in Fig. 14, but for winter.[Title Page](#)[Abstract](#)[Introduction](#)[Conclusions](#)[References](#)[Tables](#)[Figures](#)[◀](#)[▶](#)[◀](#)[▶](#)[Back](#)[Close](#)[Full Screen / Esc](#)[Printer-friendly Version](#)[Interactive Discussion](#)